I&EC research
Industrial & Engineering Chemistry Research
pubs.acs.org/IECR
Article

Structure–Property–Energetics Relationship of Organosulfide Capture Using Cu(I)/Cu(II)-BTC Edited by Valence Engineering

Yuxiang Chen,[¶] Dan Wang,[¶] Hao Jiang, Jialun Tan, Yang An, Yonghao Chen, Yuan Wu, Hui Sun,* Benxian Shen, Jigang Zhao,* Jichang Liu, Hao Ling, Di Wu,* Xiao Han, and Sixin Xu

Cite This: *Ind. Eng. Chem. Res.* 2021, 60, 371–377

ABSTRACT: Valence engineering of copper (Cu) within functional materials is effective to tune the performance and energetics of catalysts and sorbents. Here, by precisely controlling the Cu(II)/Cu(I) ratio employing $Na_2S_2O_3$ as the reduction agent, we synthesized a family of copper-1,3,5-benzenetricarboxylic acid (Cu-BTC) sorbents for organosulfur compound capture. Integrated X-ray absorption fine structure and density functional theory studies suggest that the atomic-level, short-range order changes caused by Cu reduction lead to simultaneous stability, affinity, and pore topology evolutions in Cu(I)/Cu(II)-BTC, which govern the sorption capacity and binding energetics of dimethyl disulfide capture. This multiscale fundamental study with both experimental and computational results highlights the power of coordination chemistry on materials engineering on atomic level.

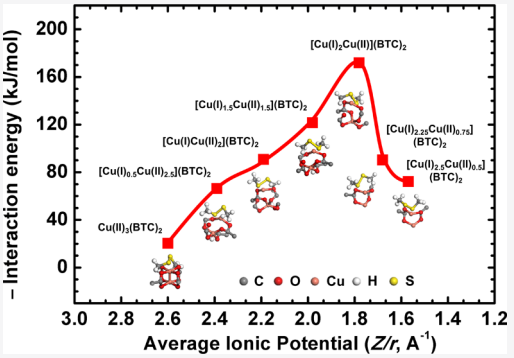

INTRODUCTION

Porous materials, such as molecular sieves,[1] metal oxides,[2] carbon-derived materials,[3] and metal–organic frameworks (MOFs),[4] play important roles in clean energy production from fossil fuels, pollutant removal, and emission control.[5−8] Tuning the metal oxidation states significantly modifies the structure, performance, and energetic stability of MOFs.[9−11] One example is that editing the ratio of Cu(I)/Cu(II) by valence engineering of copper is an effective strategy to enhance the properties of copper-based functional catalytic and separation materials.[12−16] Specifically, precise editing in the Cu(I)/Cu(II) ratio of inorganic coordination polymer quantum sheet enables high-efficiency treatment of coking wastewater.[17] The Cu(I)/Cu(II) ratio was also confirmed to be a crucial factor in determination of the activity and stability of copper-activated carbon catalysts in gas–solid acetylene dimerization reaction.[18] It is also found that the electrochemical performance of Cu-doped α-Fe_2O_3 samples was a function of Cu(I)/Cu(II) ratio, which significantly modifies the local crystal structure.[19] Moreover, Cu valence engineering has been applied to create hierarchical porosity in MOF structures to boost the performance of aromatic sulfide capture.[20]

Recently, we took advantage of valence engineering by reducing the copper in Cu-1,3,5-benzenetricarboxylic acid (BTC) from Cu(II) to Cu(I) using a series of reduction agents including ethanol, sodium thiosulfate ($Na_2S_2O_3$), hydroquinone, and glucose. We found that such controllable Cu reduction leads to stronger binding affinity (energy of adsorption), enhanced accessibility, and diffusion for selective organosulfur compound uptake.[21−23] However, the atomic level, short-range order evolution of Cu atoms remains unclear, and a comprehensive model based on integrated experimental data and computational prediction is expected to be established.

In this study, integrating X-ray absorption fine structure (XAFS) with density functional theory (DFT), we elucidated the short-range bonding evolutions of the Cu atoms. We intentionally chose dimethyl disulfide (DMDS) as the representative probe molecule for sorbent evaluation considering the multiple challenges in separation of disulfides from light petroleum products, such as low reactivity, poor dissolving activity, and weak affinity. The configurations and energetics of DMDS–Cu-BTC guest–host interactions were computationally evaluated by DFT based on the experimentally refined structural data models of Cu-BTC. Moreover, the impacts of framework topology and affinity of Cu sites on DMDS adsorption were interpreted and discussed.

EXPERIMENTAL METHODS

We systematically synthesized Cu-BTC and Cu(I)/Cu(II)-BTC sorbents using $Na_2S_2O_3$ as the reduction agent to manipulate the Cu(II)/Cu(I) ratio.[21] The synthesis procedure

Received: November 7, 2020
Revised: December 15, 2020
Accepted: December 15, 2020
Published: December 29, 2020

https://dx.doi.org/10.1021/acs.iecr.0c05483
Ind. Eng. Chem. Res. 2021, 60, 371–377

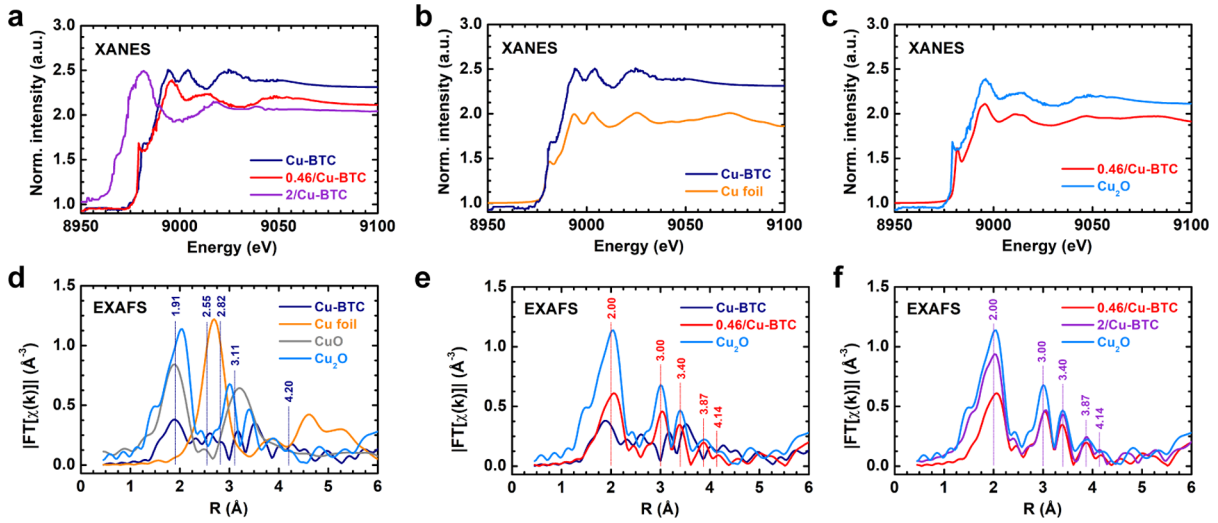

Figure 1. Cu K-edge XANES spectra of (a) Cu-BTC, 0.46/Cu-BTC, and 2/Cu-BTC; (b) Cu-BTC and (c) 0.46/Cu-BTC with background subtracted and normalized; and FTs of Cu K-edge k^3-weighted EXAFS of (d) Cu-BTC, (e) Cu-BTC and 0.46/Cu-BTC, and (f) 0.46/Cu-BTC and 2/Cu-BTC. The reference spectra of bulk Cu foil, CuO, and Cu_2O are also plotted for comparison.

is described in the Supporting Information. Here, our samples are labeled x/Cu-BTC. x is the S/Cu molar ratio we used in the post-synthesis reduction process. The XAFS data (Cu K-edge, fluorescence mode) were collected at room temperature at the Beamline 14W1 of Shanghai Synchrotron Radiation Facility (SSRF), which was equipped with a Si(311) double-crystal monochromator. Photon energy calibration was performed by setting the first inflection point energy of Cu foil as 8980 eV.[24] The storage ring was operated at 3.5 GeV between 200 and 300 mA with a cutoff at 22.5 keV. The incident beam intensity was quantified with an ionization chamber with Ar (25%) and N_2 (75%). A Lytle detector containing pure Ar was employed to record the fluorescence signals. We used Athena and Artemis interfaces of IFFEFIT for data analysis.[25,26] Specifically, we subtracted the background spectrum with a linearly equation below the absorption edge, and a polynomial of degree 2 fitted to the extended X-ray absorption fine structure (EXAFS) region. The resulting spectra were normalized using a cubic spline method with the two scans merged. Subsequently, the EXAFS oscillations, $\chi(k)$, were extracted and converted from k-space (k^2, k_{min} = 2.5 Å^{-1}, k_{max} = 10.0 Å^{-1}) to R-space with a Hanning window for radial structure function (RSF). EXAFS of the first shell was derived using inverse Fourier transform (FT) of RSF, which was further fitted using the single scattering EXAFS equation in k- and R-space. N_2 adsorption−desorption measurements were performed at 77 K with a Micromeritics ASAP 2020 V4.00 system (Norcross, GA, United States) for surface and pore structure analyses. We degassed the samples at 423 K for 12 h to clean the sample surface prior to each experiment.

Density Functional Theory. We carried out DFT simulation using Dmol3 in Materials Studio 6.1, in which high-accuracy Perdew−Burke−Ernzerhof (PBE) functional of generalized gradient approximation was applied.[27,28] Additionally, the DFT semicore pseudopods calculation was conducted using the double numerical plus polarization function. The geometric optimization was achieved by converging system energy, force, and displacement without considering symmetry restriction.

We define the energy of DMDS−Cu-BTC interactions, E_{in}, with eq 1.

$$E_{in} = E_{guest-host} - E_{guest} - E_{host} \quad (1)$$

Here, $E_{guest-host}$ is defined as the energy of guest−host interactions. E_{guest} and E_{host} represent the energy of DMDS and Cu-BTC, respectively. All the three terms share the same unit, eV. Exothermic energy of interactions suggests energetically favorable binding or guest−host interactions.

RESULTS AND DISCUSSION

We used $Na_2S_2O_3$ as a mild reducing agent for controllable modification of the copper oxidation state in Cu(II)-BTC. Conversion of Cu(II) to Cu(I) results in compositional, structural, and binding affinity modifications leading to largely fluctuant sulfide adsorption.[21] Three Cu-BTC samples with different Cu(I)/Cu(II) ratios were synthesized. Other than the parent Cu(II)-BTC with only Cu(II), we prepared two samples by post-synthesis Cu reduction using $Na_2S_2O_3$ as the reducing agent. The samples treated with S/Cu ratios = 0.46 and 2 were denoted as 0.46/Cu-BTC and 2/Cu-BTC, respectively. According to the characterizations results we reported earlier, the Cu(I) to Cu(II) molar ratios of 0.46/Cu-BTC and 2/Cu-BTC are 1.79 and 2.75, respectively (see Figure S1a). The X-ray diffraction (XRD) patterns in Figure S1b suggest that 0.46/Cu-BTC retains its characteristic framework topology, while 2/Cu-BTC presents significant structural degradation suggesting an interrupted long-range order caused by severe copper reduction. The Raman results support these structural evolutions (see Figure S1c). The evolving peaks at 275, 448, and 503 cm^{-1} reflect the Cu−O vibration changes because of reduction from Cu(II) to Cu(I).[29] In addition, one additional peak at 31.9° is observed for both 0.46/Cu-BTC and 2/Cu-BTC, the evidence of O-coordinated Cu(I) upon Cu(II) reduction.[29]

To further elucidate the atomic-scale transitions of short-range order, XAFS analyses were performed at the Cu K-edge under a continuous gas flow of argon. X-ray absorption near-edge structure (XANES) enables deep insights into the evolutions of coordination and valence of Cu in Cu-BTC upon $Na_2S_2O_3$ reduction (see Figure 1). The XANES of both Cu-BTC and 0.46/Cu-BTC feature steep increase in the white line intensity at about 8980 eV. These sharp peaks at the

https://dx.doi.org/10.1021/acs.iecr.0c05483
Ind. Eng. Chem. Res. 2021, 60, 371−377

absorption edge are associated with the 1s to 3d transition according to data collected on single crystals.[30] We also employ Cu foil, CuO, and Cu_2O as reference materials (see Figure 1). Generally, the edge positions of Cu-BTC and 0.46/Cu-BTC match well with those of Cu foil and Cu_2O, respectively (see Figure 1b,c). This is consistent with the oxidation states of Cu species determined by Raman and XPS.[21] 0.46/Cu-BTC presents a very similar spectrum as that of Cu_2O (see Figure 1c) with two peaks at 8995 and 9015 eV corresponding to Cu(I) species, whereas 2/Cu-BTC shows a distinctly different spectrum with disorder in white line and oscillations strongly suggesting a local disorder around Cu atoms caused by excessive dose of reducing agent.[31] Overall, $Na_2S_2O_3$ reduction leads to decreased Cu oxidation state from divalent Cu(II) to monovalent Cu(I), which causes decreased short-range order around each Cu atom.

EXAFS analysis was applied to determine the coordination modes of Cu species and to reveal the details of local structure evolutions due to reduction. The data obtained are fitted to the shortest backscatter distance around the Cu absorber (first Cu−O shell). We list the coordination numbers (CN), scattering path radius (R), and Debye−Waller factors (σ^2 or DWF) of all samples studied in Table 1. Specifically, the first-shell fits of the Cu−O shell EXAFS spectra are plotted in Figure S2. The Fourier transformed spectrum of Cu-BTC in Figure 1d suggests a main backscattering shell at 1.91 ± 0.02 Å, corresponding to the Cu−O shell with an average CN of 3.85 ± 0.4. This confirms that Cu is coordinated to 4 O of the trimesic acid ligands of Cu-BTC. The CNs and interatomic distances are also consistent with the Cu-BTC reference data in Cambridge Crystallographic Data Centre (CCDC).[32] Once Cu is reduced to Cu(I), the main backscattering of Cu−O decreases to 2.00 ± 0.02 Å for both 0.46/Cu-BTC and 2/Cu-BTC accompanied with significantly decreased average CNs of 3.05 ± 0.3 for 0.46/Cu-BTC and 1.90 ± 0.2 for 2/Cu-BTC (see Figure 1e,f). In addition, the DWFs (σ^2) for the first coordination shells of Cu-BTC, 0.46/Cu-BTC, and 2/Cu-BTC are 0.0005, 0.0019, and 0.0036, respectively. The increased DWFs (σ^2) suggest a decreased short-range order around the Cu atoms as they are reduced, as seen in the XANES and Raman results in Figures 1a and S1c. The atomic-scale transitions in bond length and CN are responsible for the changes in long-range order. Specifically, as CN decreases from 4 for Cu-BTC to 3 for 0.46/Cu-BTC, the number of Cu−O bond in 0.46/Cu-BTC and its length both decrease, resulting in more sites to bind sulfur species. Further decrease in CN to 2 for 2/Cu-BTC increases the number of broken Cu−O bonds, which lead to structural degradation from an open stereoscopic framework (three-dimensional or 3D) to an expanded structure (two-dimensional or 2D) (see Figure 2). Hence, despite increased number of sites for sulfide binding when we create more undercoordinated copper ions, Cu(I) enrichment leads to degradation in long-range order and much less open framework topology, both of which are counterproductive for sulfide removal.

Table 1. CN, Path Radius (R), and Mean-Squared Relative Displacements (σ^2) of all Samples Determined by EXAFS

samples	no. shells	CN	R (Å)	σ^2 (Å^2)	R factor
Cu-BTC	1st	3.85	1.91	0.0005	0.0012
0.46/Cu-BTC	1st	3.05	2.00	0.0019	0.0001
2/Cu-BTC	1st	1.90	2.00	0.0036	0.0007

Computationally, we used the distance function of DFT to quantify the distance between Cu and other atoms (see Figure 2). The simulated configurations were correlated with the experimental data. Specifically, for Cu-BTC, a strong absorption band centered at about 1.91 Å in the Fourier transformed spectrum corresponds to O shell. A similar characteristic peak with identical bond length was also observed for the CuO reference (Figure 1d), which strongly suggests that the Cu−O bond within Cu-BTC is similar as that in the CuO reference. Distance function synchronizes with the experimental results by returning a Cu−O bond length of 1.935 Å. The peak of Cu−Cu bond at 2.55 Å in the Cu-BTC spectrum (simulated at 2.47 Å) is in good accordance with that of the Cu foil reference (~2.50 Å).[33] Moreover, the peaks at 2.82 and 3.11 Å reflect the interatomic distance between Cu and C atoms. These values are consistent with the simulation results, suggesting that the unbonded Cu and C atoms are 2.799 and 3.06 Å apart. Additionally, the peak at 4.20 Å (4.188 Å simulated) is ascribed to the Cu−C interatomic distance in the Cu-BTC structure. Several low intensity peaks representing distances between the Cu atom and O or H atoms due to absorbed water molecules are not discussed. Considering the very minor contributions of these peaks indicating interatomic distances longer than 5 Å, low coordination, and high disorder, we do not focus on them in the EXAFS analyses.

Interestingly, the EXAFS peaks of reduced Cu-BTC samples disappear or shift to new positions (see Figure 1e). Specifically, the Cu-BTC peak at 1.91 Å shifts to 2.00 Å with increased intensity for 0.46/Cu-BTC, which suggests increased Cu−O bond length simulated to be 1.949 Å. The absence of peak at 2.55 Å implies broken Cu−Cu bonds within 0.46/Cu-BTC,

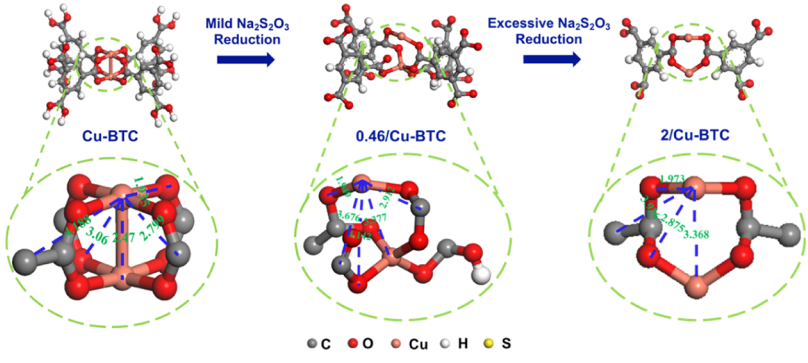

Figure 2. Structural evolution of Cu-BTC upon $Na_2S_2O_3$ reduction. The length of each bond or interatomic distance are noted (Å).

https://dx.doi.org/10.1021/acs.iecr.0c05483
Ind. Eng. Chem. Res. 2021, 60, 371−377

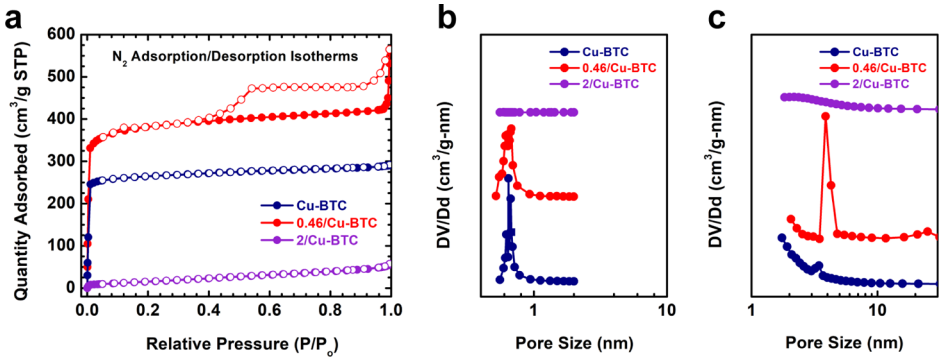

Figure 3. (a) N_2 adsorption−desorption full isotherms at 77 K and (b) microporosity and (c) mesoporosity distribution of all Cu(I)/Cu(II)-BTC samples.

which is well supported by the missing absorption of Cu−Cu stretching vibration in the Raman spectra of $Na_2S_2O_3$-reduced samples (see Figure S1c).[21] The peaks at 3.00, 3.40, and 3.87 Å are ascribed to the interatomic distance between the Cu atom and its adjacent unbonded O, Cu, and H atoms, respectively. These bond lengths are in excellent accordance with the calculated values of 2.912, 3.398, and 3.840 Å, respectively. Interestingly, a new peak at 4.14 Å emerges, which reflects the distance between the Cu atom and the H bonded to O. Besides, the peak positions of 2/Cu-BTC are nearly identical as those of 0.46/Cu-BTC yet with higher intensity. The optimized structure model of 2/Cu-BTC has a Cu−O bond length of 1.973 Å (see Figure 2) in agreement with the peak observed at 2.00 Å in the Fourier-transformed spectrum. In addition, the simulated interatomic distances between the Cu atom and its unbonded O, Cu, and H atom neighbors are 2.875, 3.368, and 3.936 Å, mirroring the experimental data at 3.00, 3.40, and 3.87 Å in Figure 1f, respectively. Moreover, the simulated interatomic distances in energy-optimized structure models agree well with the EXAFS data, which further confirm the well-defined structures of 0.46/Cu-BTC and 2/Cu-BTC. In sum, integrating EXAFS and DFT, we demonstrate that employing $Na_2S_2O_3$ as the reducing agent, we are able to manipulate the oxidation states, CNs, and bonding specifics of Cu species at atomic scale to fine-tune the local environment for expected organosulfide capture.

The impacts in Cu-BTC pore structure as the Cu(I)/Cu(II) ratio varies were evaluated using N_2 adsorption−desorption isotherm analysis at 77 K. The parent Cu(II)-BTC has type I isotherm evidencing microporosity (see Figure 3a,b). $Na_2S_2O_3$ reduction leads to decreased CN for 0.46/Cu-BTC, which enables a more open framework structure. In Figure 3a, a large hysteresis loop is observed on the isotherm of 0.46/Cu-BTC, and the pore size distribution plot suggests its mesopore span from 3 to 4 nm (see Figure 3c). In sharp contrast, because of structural degradation caused by over-reduction, significant porosity reduction is observed on 2/Cu-BTC. The simulated configuration of its collapsed structure is shown in Figure 2. Therefore, Cu(I) enrichment increases the accessibility of binding sites within Cu(I)/Cu(II)-BTC, leading to performance enhancement as we reported earlier, until the collapse of the framework structure.[21]

According to the DMDS uptakes on samples with different Cu(I)/Cu(II) ratios at 293 K,[21] the moderately reduced 0.46/Cu-BTC has boosted DMDS loading of 146.66 mg-S/g, which is about 17 times that of chemical liquid deposition-modified ZSM-5 and nearly 2 times higher than that of Ag-exchanged ZSM-5.[34,35] This value nearly doubles that of the parent Cu(II)-BTC sample (89.23 mg-S/g). In contrast, the over-reduced sample, 2/Cu-BTC, suffers from structural degradation, exhibiting decreased DMDS adsorption capability (17.81 mg-S/g). Very recently, Qi et al. report that vapor reduction is effective to generate mesoscale channels within Cu-BTC crystals.[20] Such hierarchical mesoscale porosity was confirmed to facilitate enhanced thiophene adsorption. Here, we observe a similar increase in organosulfur uptake. Furthermore, we found that microporous Cu-BTC samples modified with ethanol and glucose as the reducing agents exhibit significantly increased sorption capacity of sulfide compounds, including DMDS, ethyl sulfide, and 1-propanethiol.[23] Such evidence strongly suggests that it is the complex integration of increased binding site affinity from Cu(I) and more open pore structure prior to pore collapse that lead to the sulfide uptake boost on Cu(I)/Cu(II)-BTC. This motivates us to carry out DFT simulation to elucidate the affinity of binding sites toward sulfides, such as DMDS, as the magnitude of Cu(I)/Cu(II) increases.

DFT simulation was performed for DMDS adsorption on Cu-BTC with different Cu(I)/Cu(II) ratios. We constructed a series of Cu-BTC unit cells (see their geometries in Figure S3), each with 24 Cu atoms. Specifically, at Cu(I)/Cu(II) = 0/24, 4/20, 8/16, 12/12, 16/8, 18/6, and 20/4, their stoichiometries are $Cu(II)_3(BTC)_2$, $[Cu(I)_{0.5}Cu(II)_{2.5}]H_{0.5}(BTC)_2$, $[Cu(I)Cu(II)_2]H(BTC)_2$, $[Cu(I)_{1.5}Cu(II)_{1.5}]H_{1.5}(BTC)_2$, $[Cu(I)_2Cu(II)]H_2(BTC)_2$, $[Cu(I)_{2.25}Cu(II)_{0.75}]H_{2.25}(BTC)_2$, and $[Cu(I)_{2.5}Cu(II)_{0.5}]H_{2.5}(BTC)_2$, respectively. Here, $Cu(II)_3(BTC)_2$, $[Cu(I)_2Cu(II)]H_2(BTC)_2$, and $[Cu(I)_{2.5}Cu(II)_{0.5}]H_{2.5}(BTC)_2$ mimic the parent Cu(II)-BTC, 0.46/Cu-BTC [Cu(I)/Cu(II) ratio = 1.79] and 2/Cu-BTC [Cu(I)/Cu(II) ratio = 2.75] in our experimental studies, respectively. The calculated DMDS−Cu(I)/Cu(II)-BTC interaction energies are plotted against the average ion potential of cations (Z/r, defined as $\sum X_i(Z/r)/\sum X_i$), in which X is mole fraction, Z is charge, and r is ionic radius (see Figure 4). As the Cu(I) content increases Z/r decreases. Specifically, $Cu(II)_3(BTC)_2$ has the least favorable binding of −20.28 kJ/mol-DMDS, while the DMDS−Cu(I)/Cu(II)-BTC interactions tend to be stronger as Z/r decreases with $[Cu(I)_2Cu(II)]H_2(BTC)_2$ presenting the strongest binding of −171.87 kJ/mol-DMDS. A subsequent decrease in Z/r results in weakening adsorbate−adsorbent interactions for $[Cu(I)_{2.25}Cu(II)_{0.75}]H_{2.25}(BTC)_2$ (−90.35 kJ/mol-DMDS) and $[Cu(I)_{2.5}Cu(II)_{0.5}]H_{2.5}(BTC)_2$ (−72.16 kJ/mol-DMDS). Such "volcano plot-like" of guest−host interaction energy as a function of Z/r is consistent with

https://dx.doi.org/10.1021/acs.iecr.0c05483
Ind. Eng. Chem. Res. 2021, 60, 371−377

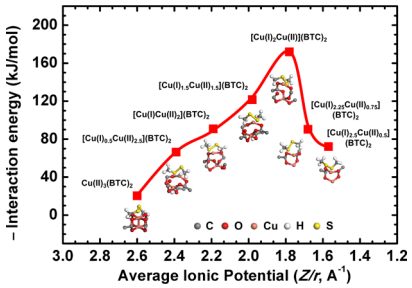

Figure 4. DMDS–Cu(I)/Cu(II)-BTC interaction energies as the average ionic potential (Z/r) varies.

our earlier report on DMDS adsorption into Cu(I)/Cu(II)-BTC,[21] in which we demonstrated that Cu(I) generated preferentially binds to sulfide molecules via strong π-complexation interactions.[36] In this study, we further our understanding with atomic-scale XAFS data and DFT insights, which strongly suggest that increase in Cu(I) concentration leads to enhanced DMDS adsorption capacity on Cu(I)/Cu(II)-BTC. Moreover, DFT simulation suggests increased DMDS–Cu(I)/Cu(II)-BTC interaction energy until the Cu(I)/Cu(II) ratio is too high to maintain the stability of an intact open framework structure. For example, Cu(I)/Cu(II)-BTC with Cu(I)/Cu(II) ratio higher than 2 results in wakened interactions, as observed on $[Cu(I)_{2.25}Cu(II)_{0.75}]H_{2.25}(BTC)_2$ and $[Cu(I)_{2.5}Cu(II)_{0.5}]$-$(BTC)_2$.

CONCLUSIONS

In conclusion, valence engineering of Cu in Cu-BTC using $Na_2S_2O_3$ leads to significantly increased DMDS loading. The XRD, Raman, XPS, XAFS results, and DFT simulation all point out that Cu valence engineering results in complex interrelated evolutions in structure–property–energetics relations. In addition, such modification causes increased DMDS adsorption performance. Specifically, 0.46/Cu-BTC with Cu(I)/Cu(II) = 1.79 presents the highest capacity (146.66 mg-S/g). Moreover, XAFS analysis reveals that the increased degree of undersaturation in Cu CN boosts the DMDS adsorption capacity and affinity. Simultaneously, DFT simulation demonstrates that $[Cu(I)_2Cu(II)](BTC)_2$ has the strongest interactions with DMDS (−171.87 kJ/mol-DMDS), which is enabled by the synergistic enhanced binding affinity and more accessible mesoporous porosity. This fundamental study demonstrates that transition metal valence engineering is an effective strategy to tune the structures of MOF-based sorbent materials with desired stability and properties.

ASSOCIATED CONTENT

Supporting Information

The Supporting Information is available free of charge at https://pubs.acs.org/doi/10.1021/acs.iecr.0c05483.

XPS spectra, XRD patterns, and Raman spectra; shell fits; geometries of a series of Cu-BTC unit cells; and convergence tolerance values (PDF)

AUTHOR INFORMATION

Corresponding Authors

Hui Sun – *Petroleum Processing Research Center, School of Chemical Engineering, East China University of Science and Technology, Shanghai 200237, China; International Joint Research Center of Green Energy Chemical Engineering, East China University of Science and Technology, Shanghai 200237, China;* orcid.org/0000-0002-8544-756X; Email: sunhui@ecust.edu.cn

Jigang Zhao – *Petroleum Processing Research Center, School of Chemical Engineering, East China University of Science and Technology, Shanghai 200237, China; International Joint Research Center of Green Energy Chemical Engineering, East China University of Science and Technology, Shanghai 200237, China;* orcid.org/0000-0002-2773-7200; Email: zjg@ecust.edu.cn

Di Wu – *Alexandra Navrotsky Institute for Experimental Thermodynamics, Washington State University, Pullman, Washington 99163, United States; The Gene and Linda Voiland School of Chemical Engineering and Bioengineering, Materials Science and Engineering, and Department of Chemistry, Washington State University, Pullman, Washington 99163, United States;* orcid.org/0000-0001-6879-321X; Email: d.wu@wsu.edu

Authors

Yuxiang Chen – *Petroleum Processing Research Center, School of Chemical Engineering, East China University of Science and Technology, Shanghai 200237, China*

Dan Wang – *Petroleum Processing Research Center, School of Chemical Engineering, East China University of Science and Technology, Shanghai 200237, China*

Hao Jiang – *Petroleum Processing Research Center, School of Chemical Engineering, East China University of Science and Technology, Shanghai 200237, China*

Jialun Tan – *Petroleum Processing Research Center, School of Chemical Engineering, East China University of Science and Technology, Shanghai 200237, China*

Yang An – *Petroleum Processing Research Center, School of Chemical Engineering, East China University of Science and Technology, Shanghai 200237, China*

Yonghao Chen – *Petroleum Processing Research Center, School of Chemical Engineering, East China University of Science and Technology, Shanghai 200237, China*

Yuan Wu – *Petroleum Processing Research Center, School of Chemical Engineering, East China University of Science and Technology, Shanghai 200237, China*

Benxian Shen – *Petroleum Processing Research Center, School of Chemical Engineering, East China University of Science and Technology, Shanghai 200237, China; International Joint Research Center of Green Energy Chemical Engineering, East China University of Science and Technology, Shanghai 200237, China*

Jichang Liu – *Petroleum Processing Research Center, School of Chemical Engineering, East China University of Science and Technology, Shanghai 200237, China; International Joint Research Center of Green Energy Chemical Engineering, East China University of Science and Technology, Shanghai 200237, China;* orcid.org/0000-0002-5295-1778

Hao Ling – *Petroleum Processing Research Center, School of Chemical Engineering, East China University of Science and Technology, Shanghai 200237, China; International Joint Research Center of Green Energy Chemical Engineering, East China University of Science and Technology, Shanghai 200237, China*

Xiao Han – *Petroleum Processing Research Center, School of Chemical Engineering, East China University of Science and Technology, Shanghai 200237, China*

https://dx.doi.org/10.1021/acs.iecr.0c05483
Ind. Eng. Chem. Res. 2021, 60, 371–377

Sixin Xu − *Petroleum Processing Research Center, School of Chemical Engineering, East China University of Science and Technology, Shanghai 200237, China*

Complete contact information is available at: https://pubs.acs.org/10.1021/acs.iecr.0c05483

Author Contributions

[¶]Y.X.C. and D.W. contributed equally.

Notes

The authors declare no competing financial interest.

■ ACKNOWLEDGMENTS

This work is financially supported by the National Natural Science Foundation of China (grants 91634112 and 21878097) and the Natural Science Foundation of Shanghai (grant 16ZR1408100). D.W. acknowledges the institutional funds from the Gene and Linda Voiland School of Chemical Engineering and Bioengineering and the Alexandra Navrotsky Institute for Experimental Thermodynamics at Washington State University.

■ REFERENCES

(1) Roth, W. J.; Nachtigall, P.; Morris, R. E.; Čejka, J. Two-Dimensional Zeolites: Current Status and Perspectives. *Chem. Rev.* **2014**, *114*, 4807−4837.

(2) Rodriguez, J. A.; Jirsak, T.; Pérez, M.; Chaturvedi, S.; Kuhn, M.; González, L.; Maiti, A. Studies on the behavior of mixed-metal oxides and desulfurization: reaction of H_2S and SO_2 with $Cr_2O_3(0001)$, MgO(100), and $Cr_xMg_{1-x}O(100)$. *J. Am. Chem. Soc.* **2000**, *122*, 12362−12370.

(3) Lee, J.-S. M.; Briggs, M. E.; Hu, C.-C.; Cooper, A. I. Controlling electric double-layer capacitance and pseudocapacitance in heteroatom-doped carbons derived from hypercrosslinked microporous polymers. *Nano Energy* **2018**, *46*, 277−289.

(4) Chong, S.; Thiele, G.; Kim, J. Excavating hidden adsorption sites in metal-organic frameworks using rational defect engineering. *Nat. Commun.* **2017**, *8*, 1539.

(5) Li, Y.; Yang, Z.; Wang, Y.; Bai, Z.; Zheng, T.; Dai, X.; Liu, S.; Gui, D.; Liu, W.; Chen, M.; Chen, L.; Diwu, J.; Zhu, L.; Zhou, R.; Chai, Z.; Albrecht-Schmitt, T.; Wang, S. A mesoporous cationic thorium-organic framework that rapidly traps anionic persistent organic pollutants. *Nat. Commun.* **2017**, *8*, 1354.

(6) Vellingiri, K.; Deep, A.; Kim, K.-H. Metal-Organic Frameworks as a Potential Platform for Selective Treatment of Gaseous Sulfur Compounds. *ACS Appl. Mater. Interfaces* **2016**, *8*, 29835−29857.

(7) Howarth, A. J.; Katz, M. J.; Wang, T. C.; Platero-Prats, A. E.; Chapman, K. W.; Hupp, J. T.; Farha, O. K. High efficiency adsorption and removal of selenate and selenite from water using metal-organic frameworks. *J. Am. Chem. Soc.* **2015**, *137*, 7488−7494.

(8) Shi, Z.; Tao, Y.; Wu, J.; Zhang, C.; He, H. L.; Long, L. L.; Lee, Y. J.; Li, T.; Zhang, Y. B. Robust Metal-Triazolate Frameworks for CO2 Capture from Flue Gas. *J. Am. Chem. Soc.* **2020**, *142*, 2750−2754.

(9) Vitillo, J. G.; Regli, L.; Chavan, S.; Ricchiardi, G.; Spoto, G.; Dietzel, P. D. C.; Bordiga, S.; Zecchina, A. Role of exposed metal sites in hydrogen storage in MOFs. *J. Am. Chem. Soc.* **2008**, *130*, 8386−8396.

(10) Chen, H.; Liu, Y.; Cai, T.; Dong, W.; Tang, L.; Xia, X.; Wang, L.; Li, T. Boosting photocatalytic performance in mixed-valence MIL-53(Fe) by changing Fe^{II}/Fe^{III} ratio. *ACS Appl. Mater. Interfaces* **2019**, *11*, 28791−28800.

(11) Tadokoro, M.; Hosoda, H.; Inoue, T.; Murayama, A.; Noguchi, K.; Iioka, A.; Nishimura, R.; Itoh, M.; Sugaya, T.; Kamebuchi, H.; Haga, M.-a. Synchronized collective proton-assisted electron transfer in solid state by hydrogen-bonding Ru(II)/Ru(III) mixed-valence molecular crystals. *Inorg. Chem.* **2017**, *56*, 8513−8526.

(12) Bai, R.; Zhang, G.; Yi, H.; Huang, Z.; Qi, X.; Liu, C.; Miller, J. T.; Kropf, A. J.; Bunel, E. E.; Lan, Y.; Lei, A. Cu(II)-Cu(I) synergistic cooperation to lead the alkyne C−H activation. *J. Am. Chem. Soc.* **2014**, *136*, 16760−16763.

(13) Allen, S. E.; Walvoord, R. R.; Padilla-Salinas, R.; Kozlowski, M. C. Aerobic copper-catalyzed organic reactions. *Chem. Rev.* **2013**, *113*, 6234−6458.

(14) Song, Y.; Fan, R.-Q.; Xing, K.; Du, X.; Su, T.; Wang, P.; Yang, Y.-L. Insight into the controllable synthesis of Cu(I)/Cu(II) metal-organic complexes: size-exclusive selective dye adsorption and semiconductor properties. *Cryst. Growth Des.* **2017**, *17*, 2549−2559.

(15) Tsai, M.-L.; Hadt, R. G.; Vanelderen, P.; Sels, B. F.; Schoonheydt, R. A.; Solomon, E. I. $[Cu_2O]^{2+}$ active site formation in Cu-ZSM-5: geometric and electronic structure requirements for N_2O activation. *J. Am. Chem. Soc.* **2014**, *136*, 3522−3529.

(16) Drake, I. J.; Zhang, Y.; Briggs, D.; Lim, B.; Chau, T.; Bell, A. T. The local environment of Cu^+ in Cu-Y zeolite and its relationship to the synthesis of dimethyl carbonate. *J. Phys. Chem. B* **2006**, *110*, 11654−11664.

(17) Li, S.; Feng, Z.; Hu, Y.; Wei, C.; Wu, H.; Huang, J. In-Situ synthesis and high-efficiency photocatalytic performance of Cu(I)/Cu(II) inorganic coordination polymer quantum sheets. *Inorg. Chem.* **2018**, *57*, 13289−13295.

(18) Li, C.; Luo, J.; Zhang, Q.; Xie, J.; Zhang, J.; Dai, B. Cu(II)Cu(I)/AC catalysts for gas-solid acetylene dimerization. *Ind. Eng. Chem. Res.* **2020**, *59*, 110−117.

(19) Zhang, J.; Lau, V. W.-h.; Liao, C.-Z.; Wong, K. W.; Lee, G.-H.; Zou, F.; Chang, C.-K.; Sheu, H.-S.; Kang, Y.-M. Controlling the valence state of Cu dopant in α-Fe_2O_3 anodes: effects on crystal structure and the conversion reactions with alkali ions. *Chem. Mater.* **2019**, *31*, 1268−1279.

(20) Qi, S. C.; Qian, X. Y.; He, Q. X.; Miao, K. J.; Jiang, Y.; Tan, P.; Liu, X. Q.; Sun, L. B. Generation of hierarchical porosity in metal-organic frameworks by the modulation of cation valence. *Angew. Chem., Int. Ed.* **2019**, *58*, 10104−10109.

(21) Wang, D.; Jiang, H.; Tan, J.; Chen, Y.; An, Y.; Chen, Y.; Wu, Y.; Liu, C.; Sun, H.; Liu, J.; Wu, D.; Shen, B. Manipulating oxidation states of copper within Cu-BTC using $Na_2S_2O_3$ as a new strategy for enhanced adsorption of sulfide. *Ind. Eng. Chem. Res.* **2019**, *58*, 19503−19510.

(22) Sun, H.; Han, X.; Liu, K.; Shen, B.; Liu, J.; Wu, D.; Shi, X. Metal-Modified Cu-BTC Acid for Highly Enhanced Adsorption of Organosulfur Species. *Ind. Eng. Chem. Res.* **2017**, *56*, 9541.

(23) Han, X. *Study on Synthesis of MOF and Its Performance for Removing Organosulfurs from Light Hydrocarbons*; East China University of Science and Technology, 2018.

(24) Sh, T.; Liu, C.-Q.; Wang, L. Antimony coordination to humic acid: Nuclear magnetic resonance and X-ray absorption fine structure spectroscopy study. *Microchem. J.* **2012**, *103*, 68−73.

(25) Webb, S. M. SIXPack a Graphical User Interface for XAS Analysis Using IFEFFIT. *Phys. Scr.* **2005**, *T115*, 1011−1014.

(26) Newville, M. IFEFFIT : interactive XAFS analysis andFEFF fitting. *J. Synchrotron Radiat.* **2001**, *8*, 322−324.

(27) Wu, X.; Ray, A. K. Density-functional study of water adsorption on the $PuO_2(110)$ surface. *Phys. Rev. B: Condens. Matter Mater. Phys.* **2002**, *65*, 085403.

(28) Boese, A. D.; Chandra, A.; Martin, J. M. L.; Marx, D. From ab initio quantum chemistry to molecular dynamics: The delicate case of hydrogen bonding in ammonia. *Chem. Phys.* **2003**, *119*, 5965.

(29) Jiang, W.-J.; Yin, Y.; Liu, X.-Q.; Yin, X.-Q.; Shi, Y.-Q.; Sun, L.-B. Fabrication of supported cuprous sites at low temperatures: an efficient, controllable strategy using vapor-induced reduction. *J. Am. Chem. Soc.* **2013**, *135*, 8137.

(30) Shulman, G. R.; Yafet, Y.; Eisenberger, P.; Blumberg, W. E. Observations and interpretation of X-Ray absorption edges in iron compounds and proteins. *Proc. Natl. Acad. Sci. U.S.A.* **1976**, *73*, 1384−1388.

(31) Grandjean, D.; Pelipenko, V.; Batyrev, E. D.; van den Heuvel, J. C.; Khassin, A. A.; Yurieva, T. M.; Weckhuysen, B. M. Dynamic Cu/

Zn interaction in SiO_2 supported methanol synthesis catalysts unraveled by in situ XAFS. *J. Phys. Chem. C* **2011**, *115*, 20175−20191.
(32) Moghadam, P. Z.; Li, A.; Wiggin, S. B.; Tao, A.; Maloney, A. G. P.; Wood, P. A.; Ward, S. C.; Fairen-Jimenez, D. Development of a Cambridge Structural Database Subset: A Collection of Metal-Organic Frameworks for Past, Present, and Future. *Chem. Mater.* **2017**, *29*, 2618−2625.
(33) Pinakidou, F.; Paloura, E. C.; Matenoglou, G. M.; Patsalas, P. Nanostructural characterization of TiN-Cu films using EXAFS spectroscopy. *Surf. Coat. Technol.* **2010**, *204*, 1933−1936.
(34) Zhao, Y.; Shen, B.; Sun, H. Chemical Liquid Deposition Modified ZSM-5 Zeolite for Adsorption Removal of Dimethyl Disulfide. *Ind. Eng. Chem. Res.* **2016**, *55*, 6475−6480.
(35) Zhao, Y.; Shen, B.; Sun, H. Adsorptive removal of dimethyl disulfide from methyl tert-butyl ether using an Ag-exchanged ZSM-5 zeolite. *RSC Adv.* **2016**, *6*, 93086−93093.
(36) Song, X.; Sun, L.; He, G.; Liu, X. Isolated Cu(i) sites supported on β-cyclodextrin: an efficient π-complexation adsorbent for thiophene capture. *Chem. Commun.* **2011**, *47*, 650.

https://dx.doi.org/10.1021/acs.iecr.0c05483
Ind. Eng. Chem. Res. 2021, 60, 371−377